PAPER A

CROSS-WELL TOMOGRAPHIC IMAGING OF GEOLOGICAL STRUCTURES IN GULF COAST SEDIMENTS

Jerry M. Harris, Gary Mavko, Daniel Moos, and Richard Nolen-Hoeksema

Seismic Tomography Project

SUMMARY

In the following case history, cross-well seismic tomography was used to successfully image both structural and stratigraphic features in Gulf Coast Miocene sediments between wells 250 feet apart. A piezoelectric downhole seismic source and three hydrophones were used to acquire the data. In addition to the targeted fault delineation, the tomography successfully imaged a number of porous sandstone layers previously identified from type logs for the Miocene. Iterative inversion was applied to a set of approximately 5500 p-wave picks. Interpretation of the resulting velocity tomogram was consistent with the pre-survey description based on well log analysis. Borehole gravity meter (BHGM) data, obtained in both wells following the tomographic survey, were used to associate density variations with the velocity features imaged by the tomography. The BHGM derived low density zones were found to coincide with the seismically imaged low velocity zones, thus supporting the identification of porous sandstone layers.

INTRODUCTION

Surface-based seismic investigations of the subsurface are inherently limited by (1) the ability to propagate energy through attenuating Earth materials, (2) the resolving power of waves, which is essentially limited to identifying features not much shorter than the seismic wavelength, and (3) the fact that sources and receivers are remote from the volume of interest. Emerging methods known as cross-well tomography, and more generally cross-well seismology, place sources and receivers at depth, closer to the reservoir or geological targets of interest and below highly attenuating near-surface materials, and thus can employ much higher frequencies of investigation (kHz) than surface seismic methods. Cross-well seismology increases the resolving power, but because energetic sources pose risks to the wellbore, limits the distance between wells at which surveys can be safely run.

Cross-well seismic tomography has been successfully used to estimate velocities between wells (Dines and Lytle, 1979; Bregman et al., 1989; and Justice et al., 1989). Although much of the tomography has been for the purposes of enhanced oil recovery (EOR), the objective in this study was to demonstrate that cross-well tomography could be used to successfully image geological features such as faults, pinchouts, or truncations. With this objective in mind, we selected a site with a series of geologic targets of interest for reservoir characterization. These include structural features such as faults and stratigraphic features such as pinch-outs or facies changes. Other features such as gas/liquid interfaces, which might exist within the zone of interest, may be imageable also.

However, these other features were not of primary interest to this study. For the selected site, the primary targets were faults within a Miocene sand/shale section onshore Gulf Coast.

A piezoelectric downhole source and a three-hydrophone array were used to acquire the data. This system of hardware provided a flexible setup for investigating the transmission properties of Gulf Coast Miocene sediments. Signals to nearly 2000 Hz were recorded at distances over 400 feet in the poorly consolidated sediments. Nearly 7000 traces of data were recorded. Of those, over 5000 p-wave traveltimes were picked and processed.

The case study reported here summarizes the steps of selecting the site, designing and executing the data acquisition plan, then processing and interpreting the data. The results are evaluated by comparing the cross-well image to our pre-survey model. Of course, there is no certainty that the pre-survey model is accurate, and thus in a sense the cross-well data can also be said to provide a test for validating the pre-survey model.

SITE SELECTION

Criteria for site selection were developed and distributed to several oil companies. The most important of these were that the primary target zone must be in a sedimentary environment and contain an isolated feature which based on available data provided sufficient velocity contrast to be imageable. We also specified that enough prior information must exist to provide an unambiguous pre-survey geological model, even though the geophysical model may not be as well defined. Three companies responded with site proposals. Amoco's Gulf Coast area #1 was selected as our first site. (The field name and precise location are confidential.)

The proposed target was at 3000 to 4000 feet within a Miocene sand/shale sequence onshore in Southeast Texas. Four wells were situated at the site within a 1000-foot radius. The closest two wellheads were about 300 feet apart (Figure 1). Each of these wells had been logged within the target zone with conductivity and SP to provide stratigraphic ties. Analysis of these data in combination with log type sections from elsewhere in the field provided a model for the proposed site which included a series of faults penetrating the region of interest. These faults were previously mapped within deeper producing horizons and their fault planes were continued upwards into the region between the proposed wells. Thus, although the precise positions of the faults as shown in Figure 1 could only be estimated based on the logs, their existence was required by previous structural analyses and reservoir characterization studies. The fault offsets were determined based on intervals within the type logs which were missing in these wells and agreed with previously known offsets within the deeper horizons.

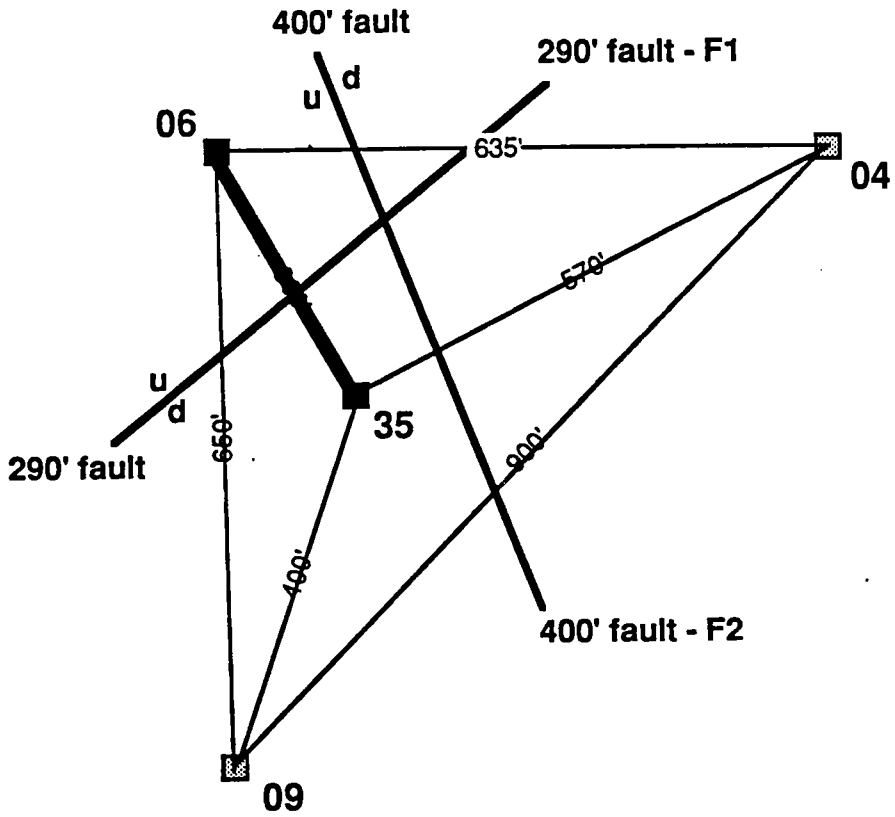

Figure 1. Plan view of study site. Faults F1 and F2 are shown at their approximate positions for a depth of 3300 feet.

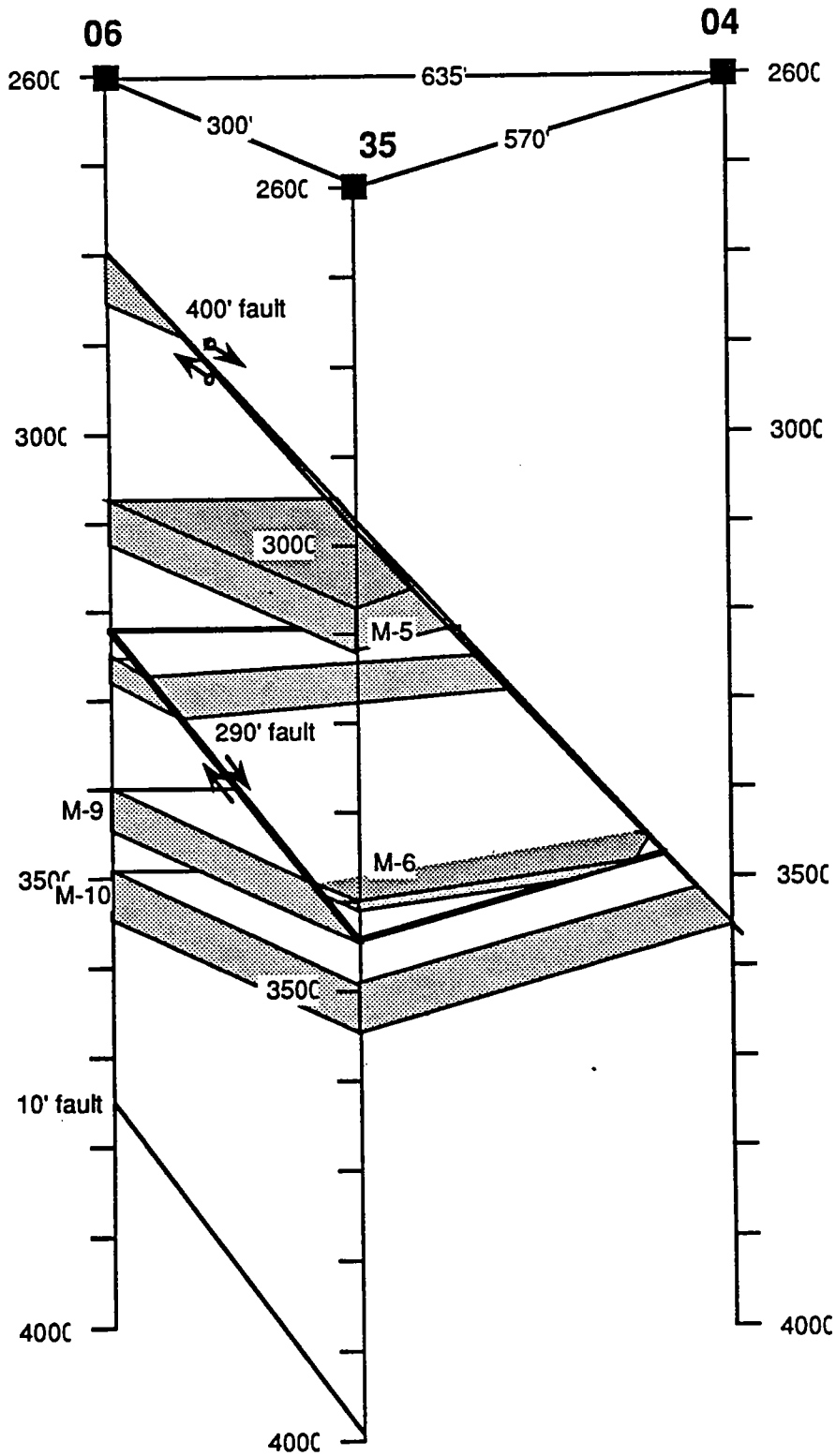

Figure 2. Interpreted pre-survey cross-section of area #1.

We chose the two closest wells (300 feet) for our first survey based on the desire to ensure that sufficient high frequency energy could be propagated between source and receivers. Four faults were identified in the section between these wells. Two of these are shown on the cross-section plotted in Figure 2. The deepest fault (not shown) has only 10' of missing section and is perpendicular to the cross-section. Proceeding up-section, the next fault (not shown) is inferred, since the M-10 to M-10A interval in both these wells is 35' too thin, relative to the type log. The existence of this fault was uncertain, as stratigraphic differences between the type well and these wells could explain the decreased thickness of these units. If the fault does exist it strikes sub-parallel to the section. The third fault (labelled F1) has about 290' of missing section, and strikes perpendicular to the section. This fault juxtaposes two sands (the M-8 and M-9) against a downthrown sequence of shales. The uppermost fault (labelled F2) removes 400' of section and is a major structural feature of the field. The fault F2 strikes sub-parallel to the section, and its location was poorly defined. The fault F1, at depths between about 3200 feet and 3450 feet, was chosen as the target of this experiment.

The physical properties of the sand/shale sequence are not well known. A density/-porosity well logging combination run in one of the wells yielded average sand densities of 2.00 to 2.33 gm/cc, and for the shales of 2.18 to 2.60 gm/cc. No velocity logs were available. Based on empirical relationships between density and velocity for these materials, a velocity model was constructed for the target fault, in which differences in velocity between the downthrown shales and the M-8 and M-9 sands provide the target.

EXPERIMENTAL DESIGN AND DATA ACQUISITION

The field survey used a piezoelectric bender bar downhole source constructed by Honeywell Marine Systems. Two bars were assembled and driven in phase to produce a source with a dominant monopole mode of vibration for the efficient generation of p-waves. The active section of the source structure is approximately 20 inches long and has a resonant frequency of about 800 Hz in free-field water at surface temperatures and pressures. The acoustic and electrical properties of the source in open water are well characterized. Unfortunately, operation in a borehole is not so well understood. The source couples acoustic energy to the formation through the borehole fluids and operates on a standard oil field wireline.

During setup and configuration prior to recording of the actual field survey, the source was driven with wavelets having different frequencies, durations, etc. These tests were instrumental in determining the frequency passband of the rocks, signal-to-noise ratio, and data acquisition parameters such as the acceptable stacking depth. Based primarily on energy considerations which affect the speed of data acquisition and is related to limitations of the recording hardware, a sweep signal was chosen for the tomographic survey. The chosen sweep was 400 ms long with start and stop frequencies of 400 Hz and 1600 Hz, respectively. Four sweeps were stacked to form the seismic trace.

Three OAS deep ocean hydrophones were used as detectors. These were separated by 10 feet of wireline. Signals detected by the hydrophones were preamplified and filtered

downhole then transmitted analog up 7-conductor wireline to the surface for more filtering and digitizing. At the surface, the data were recorded at a sample interval of 0.1 ms using an Analogic waveform analyzer. The common receiver fan taken at a depth of 3366 feet and shown in Figure 4 is typical of the data recorded. The typical shooting pattern fixed the three hydrophones and scanned the source in an aperture of approximately +/- 250 feet or roughly +/- 45 degrees. Receiver points uniformly covered the depths of 2690 to 3980 feet at ten-foot intervals. The source point intervals ranged from 5-20 feet over depths between 2400 and 4000 feet - with the 5-ft intervals about the primary target zone of 3100 to 3500 feet. A few wide aperture scans were run to obtain high angle data for identification of possible reflections off the fault zone if present. This recording geometry provided about 6700 data traces for the entire survey. A diagram of the shooting pattern is illustrated in Figure 3. Notice that in addition to shooting the primary target zone about F1, the survey was extended well above F1 to cross F2 as well.

OTHER DATA COLLECTED

Prior to conducting the cross-well survey a series of geophysical well logs were run for the two wells through casing in the depth interval of interest (2000-4000 feet). These included natural gamma spectral, cement bond, and full waveform digital sonic logs. The cement bond log was necessary to verify that the casing was sufficiently well bonded to the formation to allow efficient transmission of energy from the wellbore source to the formation. The natural gamma log was run to provide depth ties to the earlier logs, as neither conductivity nor SP (which are routinely used in this field to locate marker sand beds) can be acquired through casing. Full waveform sonics were recorded in the hope that we could extract formation compressional wave velocities for comparison to the cross-well data.

Based on the cement bond log, the casing in each well was well-coupled to the formation. Consequently, slowness time coherence processing of the sonic waveforms in the field resulted in reasonable velocities. Comparison of the gamma log to SP and conductivity previously recorded in these wells revealed depth offsets of between 20 and 40 feet; the logs were shifted to correct for these offsets prior to interpretation. After completion of the cross-well acquisition and preliminary analysis of the data, Amoco Production Research recorded a borehole gravimetry (BHGM) survey which, when interpreted assuming flat-lying layers, results in an apparent density log.

TRAVELTIME PICKS AND DATA ANALYSIS

About 5500 first arrival times were picked for creating a velocity image from the data. A small subset (< 5%) of the traces where the arrivals could not be reliably identified were ignored.

We found that a useful way to display the traveltimes and survey geometry is to plot shot depth vs. receiver depth as shown in Figure 4. Each dot represents a recorded trace, exactly as in a "stacking chart" for surface reflection data. All of the traces along any vertical line correspond to a common source fan, and all of the traces along any horizontal

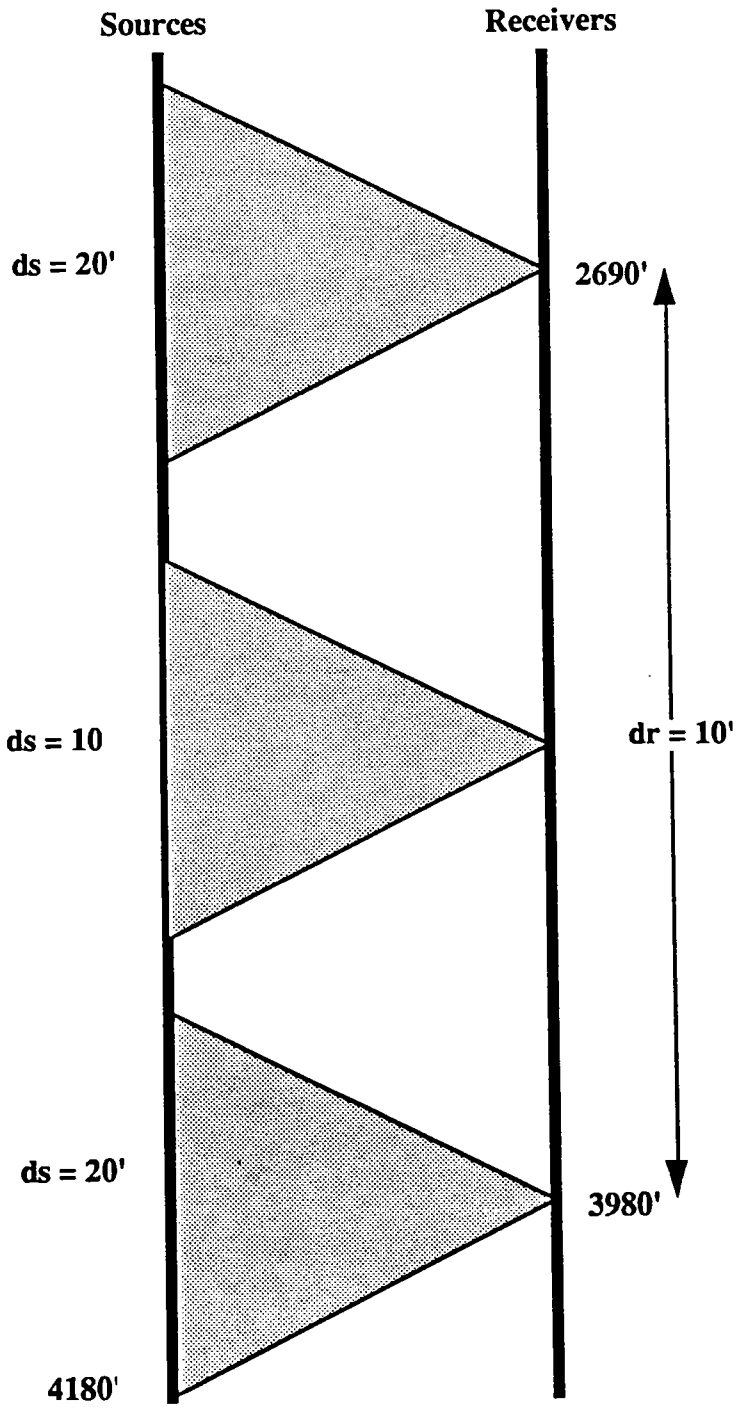

Figure 3. Overall survey geometry illustrating shooting pattern: Receivers are spaced at 10-foot intervals between 3980 feet and 2690 feet. Sources are spaced at 10-ft interval in primary target zone and 20-ft above and below target zone.

line correspond to a common receiver fan. When displayed this way, one can quickly see the fold, aperture dimensions, and variations of coverage with depth. The holes, where picks are missing, are also clearly evident.

The colors represent the picked arrival times. For more sensitivity, the times plotted here are actually the differences relative to traveltimes in a uniform velocity medium, $\Delta t = t_{pick} - r/V_0$, where t_{pick} is the picked arrival time, r is the distance between the source and receiver, and V_0 is the uniform reference velocity. Figure 5 shows the same picks interpolated to make the patterns more clear. The patterns directly indicate velocity variations in the formation between the wells. In general vertical streaks are related to near-source anomalies; horizontal streaks are related near-receiver anomalies, and streaks at other angles are related to anomalies between the wells. Source or receiver-consistent recording or geometry errors will also show up as vertical or horizontal streaks. Velocity variations with depth will show up as a color change along the center line, *source depth = receiver depth*; lateral variations will cause an asymmteric color variation with offset away from this center line. A consistent decrease of velocity with increased source-receiver offset may be an indicator of anisotropy. Please refer to the paper (Mavko and Lazaratos, 1990) in this volume for discussion on the uses of these "pick domain" plots for quality control and for interpreting velocity variations before performing an actual inversion. They also show that a first order, straight-ray tomography image is simply the "Radon transform" of the pick domain plot.

TRAVELTIME TOMOGRAPHY

The solution of the well-known non-linear inversion problem of traveltime tomography in strongly refracting media involves three distinct steps: first, we must pick observed traveltimes; second, we calculate traveltimes for an assumed slowness model; third, we invert a matrix equation where the data is given by the traveltime residuals (calculated minus observed) to obtain corrections to the assumed slowness model. Steps two and three are performed iteratively and constitute linearization of the original non-linear problem of finding both the slowness field and the raypaths. The iterations are usually stopped when an acceptable match between the calculated and the observed traveltimes is achieved. An outline of the process is shown in Figure 6.

A detailed description of the inversion procedure used on this data can be found in the paper by Harris, Lazaratos, and Michelena (1990). In brief summary, the method uses raytracing to model the traveltimes and a basis set of strings to parameterize the perturbations to the slowness field. Several general features of the inversion procedure which relate to the handling of the real data are summarized below:

Well deviation

To avoid the more complicated situation of inversion in three spatial dimensions, it is necessary to reduce the 3D deviation geometry to a plane of two dimensions. The common approach is to fix a plane intersecting the wellbores at some mean or median orientation and project all calculations of shot-receiver positions and traveltimes onto this plane. This can

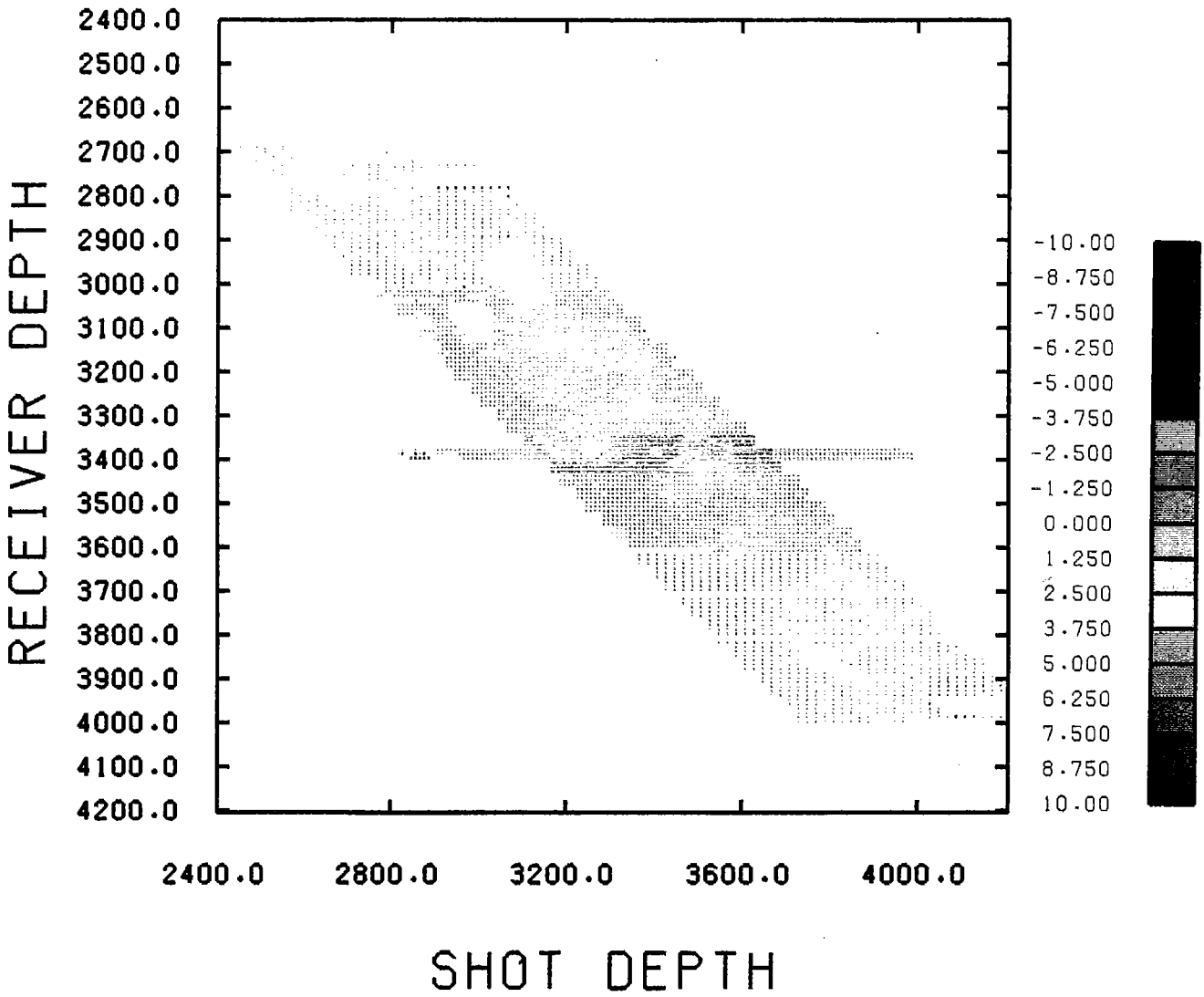

Fig. 4: Pick domain display of residual travel times (in milliseconds), showing survey geometry and rough travel time patterns.

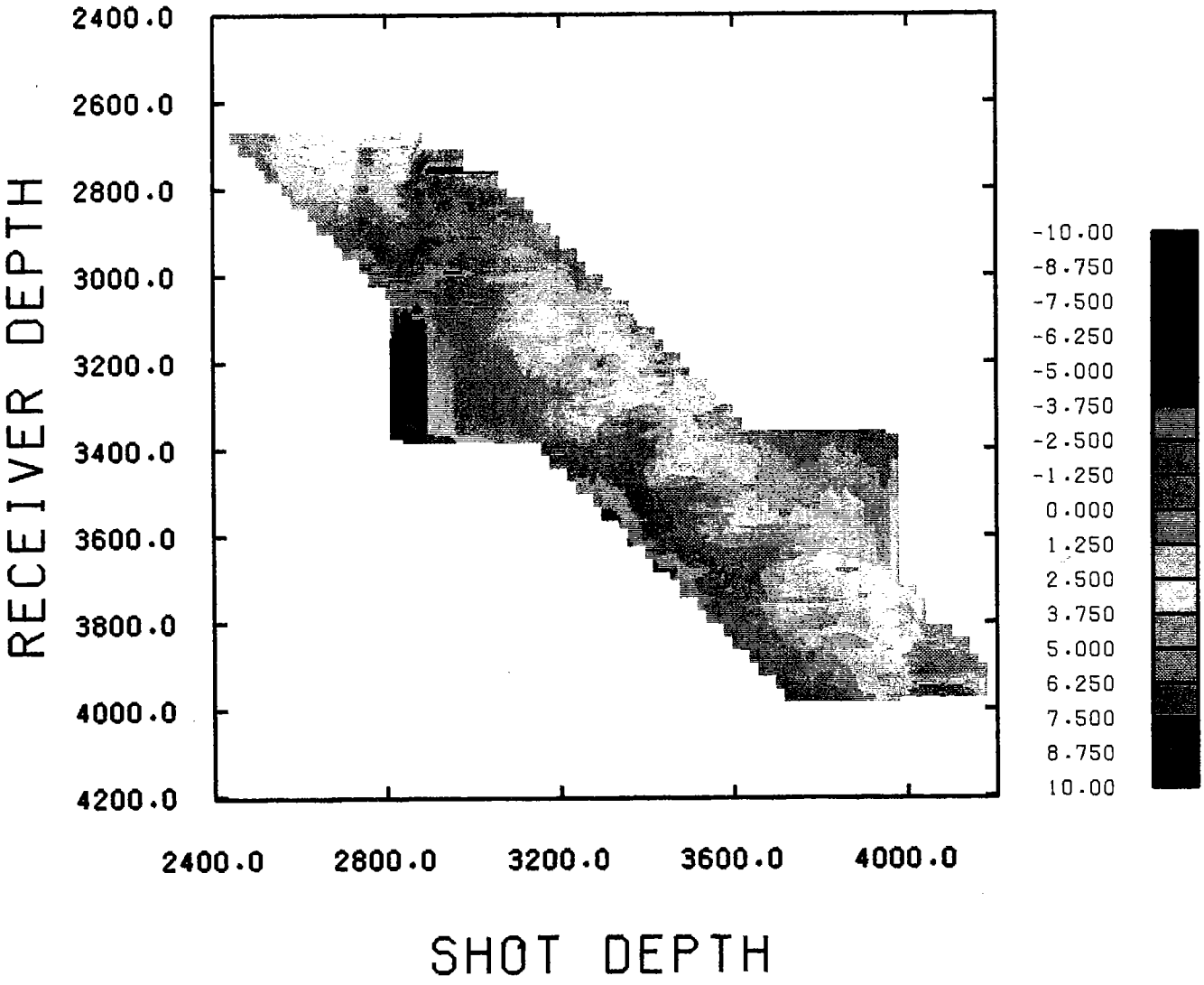

Fig. 5: Pick domain display of residual travel times, interpolated to better show the travel time patterns.

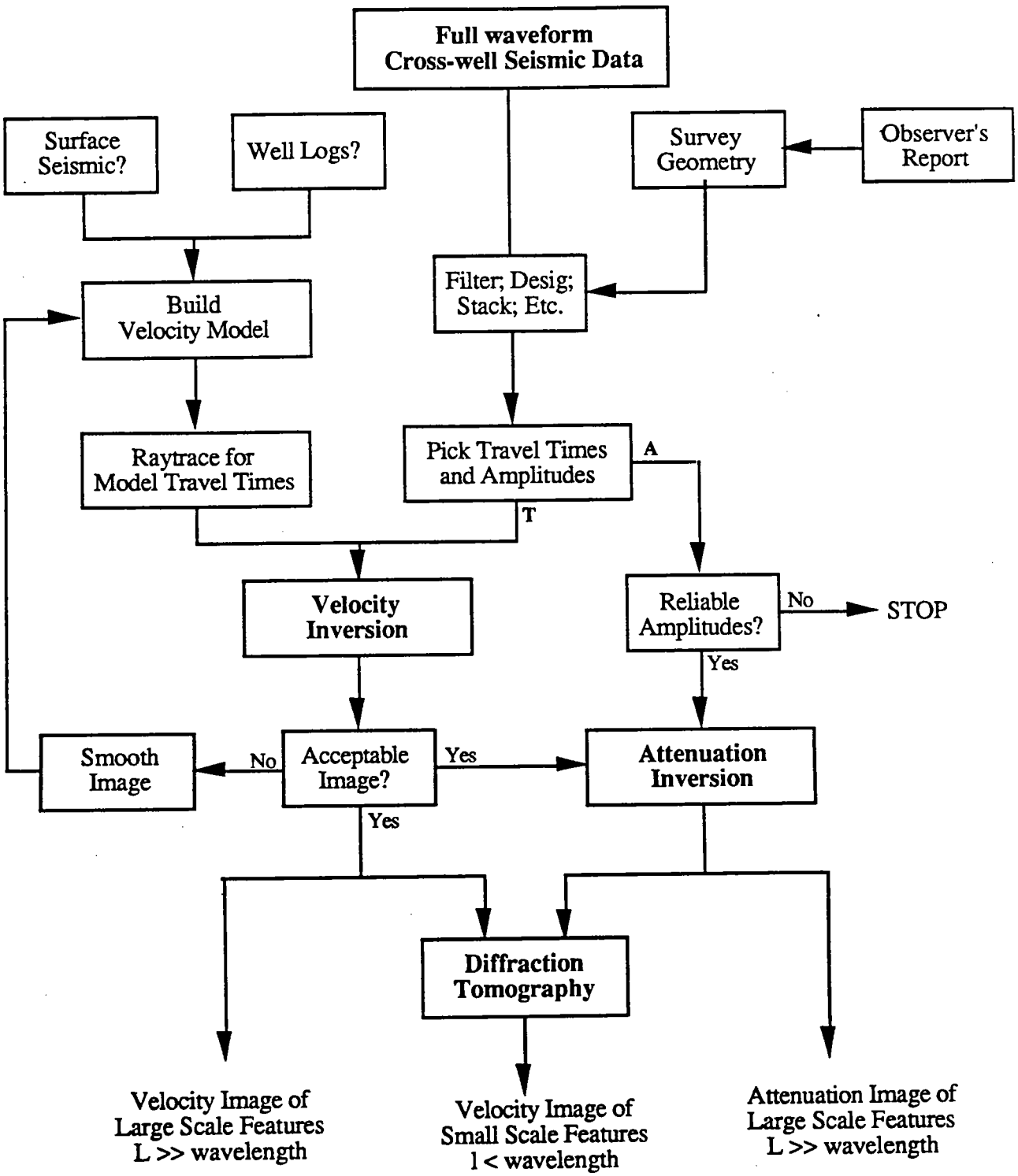

Figure 6. Schematic diagram of cross-well processing. Only traveltime processing was used on the field dataset.

result in large static corrections from the true positions to the image plane. A different approach is used here. First we note that the deviations from vertical are gradual or slowly varying; therefore, within a span of a few hundred feet, there is very little error associated with fitting a mean 2D plane to the actual deviations. Actually, we find the mean offset coordinates for each receiver point, that is, the mean orientation for the collection of shots associated with each receiver depth point. In effect, we calculate a pointing vector for each common-receiver-gather. This pointing vector then slowly rotates with depth, thus defining a local 2D plane for purposes of raytracing and inversion but varying with the actual deviation of the wells.

Raytracing

As mentioned above, raytracing is used to model albeit approximately the physical mechanism of generating the traveltimes. Calculated traveltimes are compared to observed traveltimes, thus producing a set of residuals which is inverted. This process requires calculating the traveltime for each source-detector pair or linking the source with the detector, i.e., solving the two-point boundary value problem which can be expensive and time consuming. To avoid this linking, we trace a very dense fan of rays, fit a curve through the observed common-receiver array of traveltimes, then use the curve to map observed traveltimes onto the calculated rays. This allows the raytracing to be vectorized on the computer and provides an important means of interpolation for the string-generated image.

Inversion

The inversion problem is now reduced to inverting a matrix equation relating the residual traveltimes (data) to perturbations of the assumed slowness field. For this purpose, a new procedure known as string tomography (Harris, Lazaratos, and Michelena, 1990) was used. Rather than parameterize the perturbations to the slowness field in square orthogonal pixels, this new procedure uses strings which are derived from the raypaths themselves. The approach avoids two costly operations in the inversion process, calculating elements of the projection matrix and inverting the projection matrix.

Results

String tomography was applied to the nearly 5500 traveltimes acquired during the imaging survey. The inversion procedure, outlined in Figure 6, involved several raytrace iterations. The results for two different starting models are substantially the same. See (Harris, et. al., 1990) for inversion details. The tomogram used for interpretation was generated after five iterations, starting with constant velocity slowness model. his result is shown in Figure 8. Recall the manner described above of handling the well deviations. In the tomogram display of Figure 10, well 06 is plotted straight along the vertical and all the deviation is allowed to appear in the offset well 35. Therefore, to register the coordinates to the real world, one should move down well 06 and out a radial distance toward well 35.

GEOLOGIC INTERPRETATION

Tomogram validation

Figure 7 illustrates the final velocity image overlain by the original geological model. Each of the faults predicted by the model have expressions in the final image. However, these expressions are different for the different faults. The original target of the experiment, the 290' fault labelled F1, truncates a series of beds including a very high-velocity shale below the M-8 against the overlying downfaulted shales. The position of this fault can be inferred from the bed truncations. Interestingly, the 400' fault labelled F2, which was oblique to the original section and poorly characterized in the geologic model, shows up very clearly at its predicted depth and orientation as a sharp velocity contrast, with higher velocities above than below the fault (trapped gas?). The two small offset faults below the primary target zone could also be interpreted, again based on bed truncations, but probably would not have been resolved based only on the image.

Comparisons of the tomogram to the other data

Looking in more detail at the relationship between the image and the well log data, there is a striking correlation between lithology and velocity. Figure 8a shows the image overlain by the SP logs, plotted at the locations of the wells on the image plane. Background shale readings are generally associated with intervals of higher velocity, whereas sands have distinctly lower velocities than the surrounding materials. For example, in well 06 the M-4 sand shows up as a pronounced low velocity (<7865 ft/s) interval. This sand continues across section and is similarly imaged near the 35 well. The M-9 sand, which is present in well 06 but faulted out by the 290' fault in 35, is also associated with a low velocity horizon, as are the M-10 and M-10A.

A similar comparison between the BHGM densities and the velocity image is shown in Figure 8b. Overall, low BHGM densities and low velocities are well correlated. This correlation between a deep-reading BHGM measurement and the cross-well image is a striking example of the ability of these two methods to provide valuable and complementary data. Furthermore, the congruence between low densities and low velocities generally confirms standard petrophysical assumptions. It should be noted, however, that the BHGM densities were obtained from 1-D inversion of the gravity station measurements. Differences between the resulting densities at the two wells, and the lateral discontinuities in the velocity image, suggest that the 1-D assumption is at best a first-order approximation.

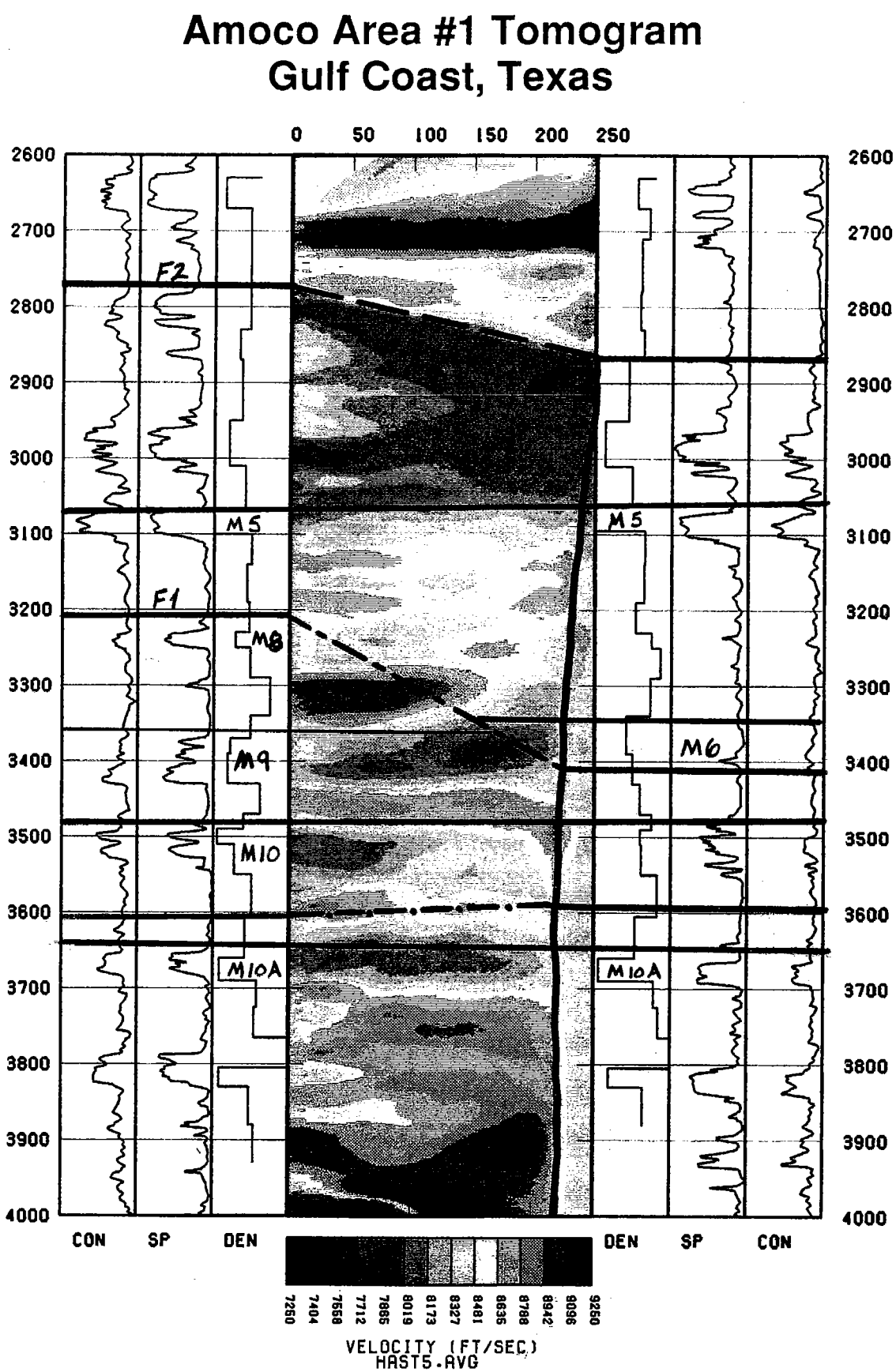

Fig. 7. Final tomogram with geological overlay.

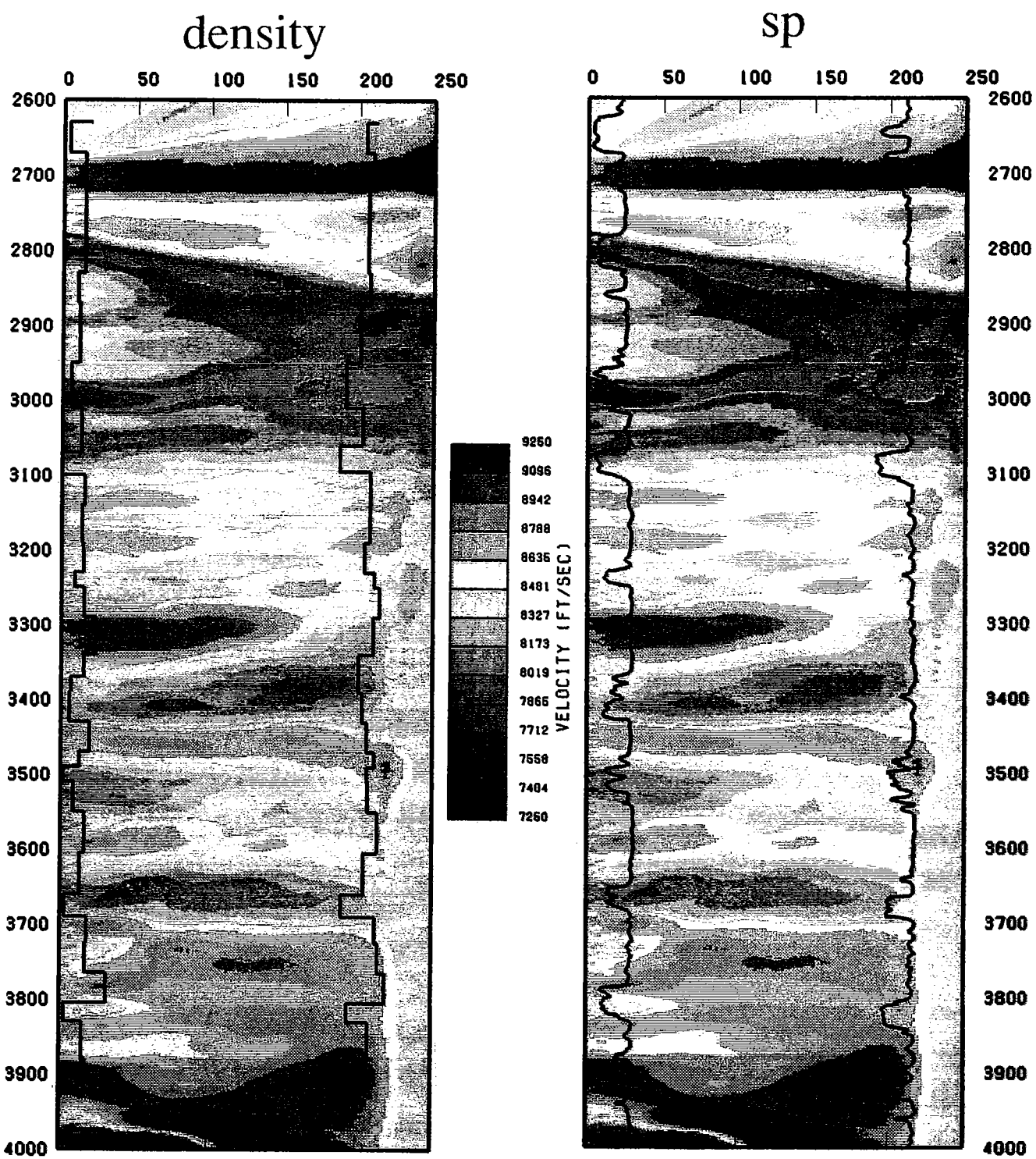

Fig. 8. Final tomogram with density and sp overlay.

In marked contrast to the expressions of the other sands, the position of the M-5 sand in the SP log is marked by a steep velocity gradient, rather than a low velocity zone. This sand is expressed in the electrical logs by a doublet (two sands separated by a less sandy unit?). Perhaps the M-5 is a permeability barrier, and the velocity gradient reflects differences in pore-fluid pressure or composition. The gravity data show that the M-5 sand has low density, similar to the densities of the other sands. Thus, the lack of a low velocity zone at the level of the M-5 may indicate that this sand is different microstructurally from the other sands in this section. This difference may also result in the M-5 acting as a permeability barrier

.

The M-10B is associated with a low velocity and density near the 06 well. Near the 35 well, the M-10B has low density and clear SP and resistivity expressions, but there is little velocity change. This lack of seismic expression may be due to lack of coverage near the bottom of the survey, or to stratigraphic microstructural changes between the two wells.

In summary, comparisons between petrophysical log data and the seismic velocity image show the synergy which can be achieved using multiple measurements. The combined data provide a consistent picture of geologic structure, and differences among these data give insight into the petrophysical properties of the individual units.

CONCLUSIONS

The results of cross-well experiments at the Southeast Texas site demonstrated the suitability of cross-well tomography for work at moderate depths and offsets in typical reservoir environments. A geologic target identified by interpretation of core and well log data and a priori structural information from log ties at other wells was successfully imaged. This is promising for two reasons. First, one never has complete confidence in well-to-well log correlations. Second, in many situations there is not enough data to produce even a testable interpretation of the structure between wells in a field.

The target was initially chosen based on the expectation that a large offset fault juxtaposed media with a pronounced velocity contrast. We imaged that target by resolving sand beds with thicknesses on the order of 15-20 feet that were truncated against a thick shale section. We also imaged two small offset faults. One of these had a throw of 35' and a strike sub-parallel to the section. The other fault had a throw of only 10' and was perpendicular to the section. Although this is a remarkable example of the ability of cross-well tomography to image features close to the wavelength of the seismic signal, it is unlikely that these features would have been interpreted based on the tomographic image alone.

The data were acquired with a high frequency piezoelectric downhole source. The frequency content of the detected seismic signal was bounded on the low end by source inefficiency and on the high end by attenuation in the Earth materials. Even so, frequencies to nearly 2000 Hz were recorded at slant path distances exceeding 400 feet. At velocities ranging down to 7000 ft/sec, this slant path distance corresponds to over 100 wavelengths.

Near wellbore low velocity intervals seen in the tomogram could be tied to individual sands identified by SP and conductivity logs. These sands had low densities relative to the surrounding shales, and therefore densities computed from borehole gravimetry correlated remarkably well with the tomographic image. Interestingly, there were similarities and differences between velocities computed from sonic waveforms recorded through casing, and cross-well seismic velocities. The differences, concentrated in a 300' depth interval, are intriguing but need verification.

We consider that the high frequency cross-well technique has been validated for these experimental conditions - that is imaging small-scale (on the order of 10-50 feet) structural features of a sand/shale sequence at moderate offsets (300 feet). We are planning further studies at the same site to extend the offset between wells, to investigate the out-of-plane 400' fault, and to allow evaluation of interpretation techniques for 3-D data.

REFERENCES

Bregman, N.D., Bailey, R.C., and Chapman, C.H., 1989, Cross-hole seismic tomography: Geophysics, 54, 200-215.

Dines, K. A., and Lytle, R. J., 1979, Computerized geophysical tomography, Proc. IEEE, 67, pp. 1065-1073.

Harris, J., Lazaratos, S., and Michelena, R., 1990, Tomographic string inversions, 1990 SEG meeting, San Francisco.

Mavko, G. and Lazaratos, S., 1990, Cross-well tomographic analysis in the pick domain, Paper C, this volume.

McMechan, G. A., Harris, J. M., and Anderson, L., 1987, Cross- well tomography for strongly variable media with application to scale model data, Bulletin of the Seismological Society of America, Vol. 77, No. 6, pp. 1945-1960.

Michelena, R, and Harris, J. M., 1990, Tomographic inversion using natural pixels, Paper F, this volume.

Justice, J. H., Vassiliou, A. A., Singh, S., Logel, J. D., Hansen, P.A., Hall, B.R., Hett, P.R., and Solanki, J.J., 1989, Acoustic tomography for monitoring enhanced oil recovery: The Leading Edge, 8, no. 2, 12-19.

ACKNOWLEDGEMENTS

The authors thank Amoco Production Company for its support in acquiring the data, and the Gas Research Institute for its financial support of the cross-well tomography project at Stanford University.